Modelling norovirus dynamics within oysters emphasises potential food safety issues associated with current testing & depuration protocols☆

Paul McMenemy [a,b,*,1], Adam Kleczkowski [a,b], Nick G.H. Taylor [c,d]

[a] *University of Strathclyde, 16 Richmond Street, Glasgow, G1 1XQ, United Kingdom*
[b] *University of Stirling, Airthrey Road, Stirling, FK9 4LA, United Kingdom*
[c] *Cefas, The Nothe, Barrack Road, Weymouth, DT4 8UB, United Kingdom*
[d] *Office for National Statistics, 2 Marsham Street, London, SW1P 4DF, United Kingdom*

ABSTRACT

Norovirus is a significant global cause of viral gastroenteritis, with raw oyster consumption often linked to such outbreaks due to their filter-feeding in harvest waters. National water quality and depuration/relaying times are often classified using *Escherichia coli*, a poor proxy for norovirus levels in shellfish. The current norovirus assay is limited to only the digestive tracts of oysters, meaning the total norovirus load of an oyster may differ from reported results. These limitations motivated this work, building upon previous modelling by the authors, and considers the sequestration of norovirus into observed and cryptic (unobservable) compartments within each oyster. Results show that total norovirus levels in shellfish batches exhibit distinct peaks during the early depuration stages, with each peak's magnitude dependent on the proportion of cryptic norovirus. These results are supported by depuration trial data and other studies, where viral levels often exhibit multiphase decays. This work's significant result is that any future norovirus legislation needs to consider not only the harvest site's water classification but also the total viral load present in oysters entering the market. We show that 62 h of depuration should be undertaken before any norovirus testing is conducted on oyster samples, being the time required for cryptic viral loads to have transited into the digestive tracts where they can be detected by current assay, or have exited the oyster.

1. Introduction

Noroviruses (NoVs) have long been identified as a significant cause of acute gastroenteritis (Bányai et al., 2018; O'Brien et al., 2018), inducing symptoms such as muscular and abdominal pain, diarrhea and nausea that can often result in dehydration (Hassard et al., 2017). Children under 5 years old are particularly vulnerable to the effects of acute gastroenteritis from NoV, with immunocompromised children especially at risk of fatal outcomes from acute gastroenteritis (Patel et al., 2008; Esposito et al., 2014; Thongprachum et al., 2013). NoVs are transmitted via faecal-oral routes, by personal contact, or from contaminated water, environment or food (O'Brien et al., 2018; Hassard et al., 2017; Lees, 2000). A major pathway from food to human is the consumption of bivalve shellfish (Lees, 2000; Greening and McCoubrey,

2010; Schaeffer et al., 2013) as they are known to bioconcentrate any pathogens that are present in their immediate waters during filter-feeding (Greening and McCoubrey, 2010; Lees, 2010; Muniain-Mujika et al., 2002; Guyader et al., 2006). The occurrence of NoV outbreaks was reported to increase before the COVID-19 pandemic (van Beek et al., 2013) and, while NoV outbreaks were reduced during 2020–21, there are indications that outbreaks are returning to pre-pandemic levels (Keaveney et al., 2022; Kambhampati et al., 2022).

Edible oysters, such as Pacific cupped (*Magallana gigas*) and American cupped (*Crassostrea virginica*) oysters, have been further identified as particular NoV transmitters due to the prevalence of their raw consumption in many countries, which poses a greater risk than the consumption of cooked produce that is contaminated with NoV (Schaeffer et al., 2013, 2018; Pouillot et al., 2021). Many oyster farms are located

in coastal waters and often close to sewage treatment works, increasing the likelihood of NoV contaminated oysters at harvest (Schaeffer et al., 2018). A 2018 survey collected oysters from various United Kingdom (UK) points-of-sale and detected NoV in 68.7% of samples (Lowther et al., 2018), thus emphasizing the importance of pathogen control measures within the shellfish industry. Most developed countries have legislation in place to minimise the levels of faecal contamination found in shellfish: the European Union currently uses a harvest site classification based on levels of an indicator organism *Escherichia coli* (*E. coli*) which identifies safe sites (Class A), sites where further shellfish purification is required (Class B, C), and sites where harvesting is not permitted (Anonymous, 2004). The UK adopted the same classification protocols when they exited the European Union in 2020 (Food Standards Agency, 2022); however, recent reports of English water companies discharging raw sewage into rivers and coastal waters (Armitage, 2022; Laville and McIntyre, 2019; Brown, 2020) could result in more sites being classified as B or C, or farming permits being rescinded.

One purification method is depuration, where harvested shellfish are submerged in tanks of clean, oxygenated water where they excrete any accumulated contaminants. Current standard depuration periods are around 42 h (Polo et al., 2014); however, this time period is based upon the removal of *E. coli* (Doré and Lees, 1995) and is often insufficient for reducing the levels of enteric viruses (such as NoV) that can persist within shellfish beyond 42 h of depuration (Lees, 2000; McMenemy et al., 2018). The most common assay employed for the detection of NoV in shellfish is polymerase chain reaction (PCR); however, this test only quantifies the NoV load within the digestive glands of the oyster (Lees, 2000; Anonymous, 2017), with the rest of the shellfish discarded including the tract of the oyster's digestive system that precedes the digestive glands (Lees, 2010; Loisy et al., 2005).

Some studies have shown that molluscs compartmentalise NoV within biological tracts that are not currently tested by PCR, and that molluscs internally sequester and transfer pathogen levels sequentially through their whole digestive system, transiting NoV through their gills, labial palps, mouth, oesophagus and intestines before reaching their stomach/digestive glands (Doré and Lees, 1995; Wang et al., 2008). Therefore, NoV levels that are not currently detectable by PCR must be considered from a food safety standpoint, as whole oysters are often consumed uncooked, exposing consumers to the entire NoV load present in the oyster and not just the load that is detectable by PCR. Therefore, it is possible that oysters contain significant levels of NoV which cannot be measured by the current PCR assay. Wang et al. carried out 2008 study, analysing the sequestration of NoV in suminoe oysters (*Crassostrea ariakensis*) using immunohistochemical analysis (Wang et al., 2008), and reported that significant NoV levels were discovered outside the digestive glands. In a similar study, Dore and Lees (Doré and Lees, 1995) analysed the depuration effect on FRNA + bacteriophage within oysters and mussels, and reported that FRNA + bacteriophage was still detected in approximately 60% of the digestive glands and 40% elsewhere within mussels after depuration. Note that, while FRNA + bacteriophage can often be used as a NoV or fecal matter test surrogate, how this pathogen bioaccumulates in oysters does differ from NoV accumulation which binds to histo-blood group antigens within the mollusc (Su et al., 2018; Leduc et al., 2020; Ma et al., 2018).

Some studies have been carried out to quantify minimum depuration periods for NoV, although there exists a paucity of *in vivo* testing of depuration NoV effectiveness (Ueki et al., 2007; Savini et al., 2009; Neish, 2013). To address this shortage, mathematical modelling of depuration effectiveness on pathogens has been undertaken, with models of NoV in single molluscs (Polo et al., 2014, 2015) and of shellfish populations during depuration (McMenemy et al., 2018). The NoV population model was founded on two main premises: (*i*) NoV levels are lognormally distributed across a molluscan population; (*ii*) each mollusc stores any pathogen in its digestive glands.

However, Rowan (2023) reported that "not all documented decontamination studies appear to exhibit viral data that are log-linear in

performance", indicating that there may be some other mechanism at play with respect to NoV levels during depuration. Data from a 2013 study by Neish (2013) indicated that median NOV levels in oysters sampled during a controlled study could increase after 50 h of depuration, or at least do not have decay profiles which are log-linear, as reported in other literature (Rowan, 2023; Rupnik et al., 2021).

These studies, along with the consideration that there may exist some cryptic (that is, unobservable by current assay) NoV sequestration within oysters, motivated this work which extends the depuration population model of McMenemy et al. (2018) by incorporating two compartments of NoV in each oyster: an observable compartment (digestive gland), and a cryptic compartment (rest of oyster) which is not currently tested for NoV by PCR. Results from the model are presented, with focus on the difference of minimum depuration times between the compartmental and non-compartmental model variants. The implications for testing protocols are then considered and discussed, and recommendations for future testing protocols are presented.

2. Model

2.1. Single oyster NoV loads

The model is constructed on the assumption of compartmentalised NoV loads as described above. Once an oyster resumes filter-feeding in a depuration tank, any NoV present in the cryptic, pre-gland parts (y_t) would begin transiting through the digestive system into the digestive gland (x_t), Fig. 1. A compartmental model can describe this process, with the total NoV load in the oyster at time t defined as z_t, where $z_t = x_t + y_t$, where the compartment x_t is referred to as the *observable* NoV load and y_t as the *cryptic* NoV load. For simplicity, it is assumed that x_t and y_t, as continuous functions of time, satisfy a set of differential equations where

$$\dot{x}_t = ky_t - bx_t, \tag{1}$$

$$\dot{y}_t = -ky_t. \tag{2}$$

The parameter k quantifies the internal transfer rate of NoV from the cryptic compartment into the observable section; the parameter b describes the rate at which NoV is removed from the digestive gland (and from the oyster) by excretion during depuration (Fig. 1).

We assume that, at $t = 0$ (pre-depuration), the total NoV load is split between these two compartments, with the observable and cryptic loads set as proportions of the total load (z_0), where $x_0 = Az_0$ and $y_0 = (1 - A) z_0$. The value of A determines the proportion of an oyster's total, initial NoV load (z_0) present in the observable part of the digestive gland, with $0 < A \leqslant 1$.

Equations (1) and (2) are first-order, homogeneous equations and solutions are readily obtained, beginning with y_t:

$$y_t = (1 - A)z_0 \exp\{-kt\}, \tag{3}$$

with the observable compartment's solution described by

$$x_t = x_0 \, \Theta_t, \tag{4}$$

where

$$\Theta_t = A^{-1} \left[\frac{k(1-A)}{(b-k)} \exp\{-kt\} + \frac{(Ab-k)}{(b-k)} \exp\{-bt\} \right], \tag{5}$$

and $0 \leqslant A \leqslant 1$, $b \neq k$. A solution for the total NoV load in an oyster (z_t) can also be obtained by substituting the equations describing x_t and y_t (Equations (3)–(5)) into $z_t = x_t + y_t$ and simplifying to obtain

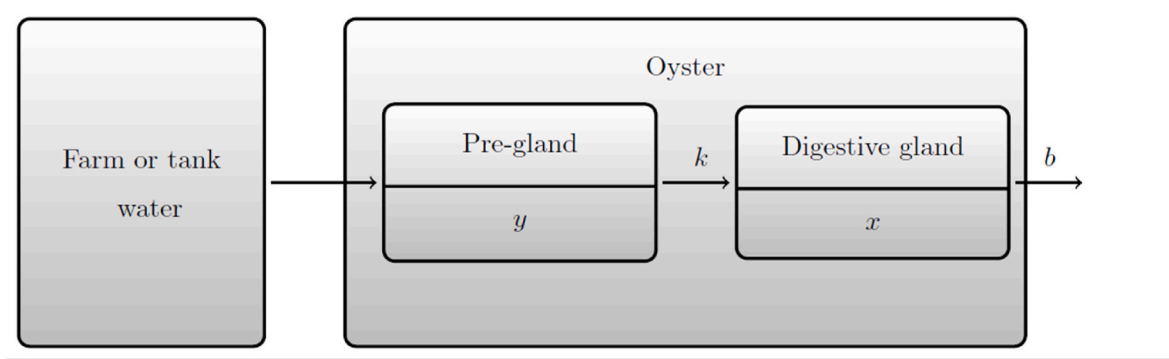$$z_t = z_0 \, \Omega_t, \tag{6}$$

where

Fig. 1. Representation of NoV transit through an oyster's digestive system during relaying/depuration.

$$\Omega_t = \left[\frac{b\,(1-A)}{(b-k)}\exp\{-kt\} + \frac{(Ab-k)}{(b-k)}\exp\{-bt\} \right]. \tag{7}$$

If $k < b$ there would be no accumulation of NoV in x_t, something which is contrary to literature findings that NoV selectively binds and aggregates within the digestive gland of molluscs (x_t) (Le Guyader et al., 2006; Ueki et al., 2007; Anonymous, 2012). Therefore, we restrict $b < k$ to describe the internal transfer of NoV from y_t to x_t. Equations (3)–(7) are derived in A Appendix.

2.2. Probability distributions of x_0 and z_0

Equations (1)–(7) describe the depuration dynamics of compartmentalised NoV within individual oysters. As described by McMenemy et al. (2018), these equations can be applied across an oyster population to construct models of the depuration process. For simplicity we assume that all variability in the system is associated with the total initial NoV loads, Z_0, and that A is fixed across the population. Thus the distribution of initial observable NoV is given by $P(X_0 = x_0) = A^{-1} P(Z_0 = z_0)$. As per McMenemy et al. and references therein (McMenemy et al., 2018), we assume that NoV loads across an oyster population are well-described by a log-normal distribution, and the probability density function (PDF) of observable loads is described by:

$$P(x_0) = \frac{1}{x_0 \sigma_0 \sqrt{2\pi}} \exp\left\{ \frac{-(\ln(x_0) - \mu_0)^2}{2\sigma_0^2} \right\}. \tag{8}$$

where μ_0 is the mean of the log-values of observable NoV per shellfish, and σ_0 the standard deviation of these values. The probability distribution of total NoV at pre-depuration can also be derived:

$$P(z_0) = \frac{1}{z_0 \sigma_0 \sqrt{2\pi}} \exp\left\{ \frac{-(\ln(A z_0) - \mu_0)^2}{2\sigma_0^2} \right\}. \tag{9}$$

Equations (8) and (9) model the pre-depuration distributions of the observable and total NoV loads, respectively.

2.3. NoV distributions during depuration

Equations (4)–(7) describe the observable and total NoV loads present in individual oysters prior to and during depuration, and can be used to change the variables of Equations (8) and (9) to obtain density functions for any time during depuration ($t \geqslant 0$). For observable NoV loads, we state the relationship between the pre-depuration NoV distribution, $P(x_0)$, and during depuration distribution, $P(x_t)$, as $P(x_0)dx_0 = P(x_t)dx_t$. Using Equations (4) and (8), we can derive $P(x_t)$ where

$$P(x_t) = \frac{1}{x_t \sigma_0 \sqrt{2\pi}} \exp\left\{ -\left(\ln\left(\frac{x_t}{\Theta_t}\right) - \mu_0 \right)^2 \Big/ 2\sigma_0^2 \right\}. \tag{10}$$

Similarly, the density function describing the total pathogen load during depuration ($P(z_t)$) can also be derived as:

$$P(z_t) = \frac{1}{z_t \sigma_0 \sqrt{2\pi}} \exp\left\{ -\left(\ln\left(\frac{A z_t}{\Omega_t}\right) - \mu_0 \right)^2 \Big/ 2\sigma_0^2 \right\}. \tag{11}$$

Thus, Equations (10) and (11), coupled with the definitions of Θ_t (Equation (5)) and Ω_t (Equation (7)), model the respective distributions of the observable and total NoV loads during the depuration process.

2.4. Minimum depuration times

McMenemy et al. (2018) applied two control parameters in their model to obtain depuration time estimates which conform to these controls:

(i) Ψ - a pathogen threshold value per shellfish;
(ii) φ - a proportion of shellfish with pathogen loads less than Ψ.

Applying the same controls to this study, the parameter Ψ splits the area under the distributions' curves into two parts: the *head* of the density distribution where $x_t, z_t < \Psi$ with an area equal to the proportion of oysters whose NoV load is less than Ψ, and the *tail* whose area represents the proportion of oysters with NoV loads greater than Ψ.

The value of φ can be stated as being, respectively for observable (Equation (10)) and total (Equation (11)) pathogen loads, the areas under the distribution curves where:

$$P(x_t < \Psi) = \int_0^{\Psi} \frac{1}{x_t \sigma_0 \sqrt{2\pi}} \exp\left\{ -\left(\ln\left(\frac{x_t}{\Theta_t}\right) - \mu_0 \right)^2 \Big/ 2\sigma_0^2 \right\} dx_t = \varphi \tag{12}$$

and

$$P(z_t < \Psi) = \int_0^{\Psi} \frac{1}{z_t \sigma_0 \sqrt{2\pi}} \exp\left\{ -\left(\ln\left(\frac{A z_t}{\Omega_t}\right) - \mu_0 \right)^2 \Big/ 2\sigma_0^2 \right\} dx_t = \varphi. \tag{13}$$

The values of the integrals in Equations (12) and (13) will equal the parameter φ only after a specific depuration time t has elapsed. A minimum depuration time (MDT) required to satisfy the constraints parameters Ψ and φ was defined by McMenemy et al. (2018) and an analytical solution for t was obtained; however, analytical solutions of Equations (12) and (13) for t cannot be derived. The terms Θ_t and Ω_t (Equations (5) and (7)) are both in the generic form $\Theta_t, \Omega_t = [m\exp\{-kt\} + n\exp\{-bt\}]$ $(m, n \in \mathbb{R})$, which have no analytical solution for t.

2.5. Variability estimation

Obtaining parameter estimates for NoV variability across shellfish populations is time-consuming (Neish, 2013). To address this issue,

McMenemy et al. (2018) derived a worst-case estimate of the variability inherent in the exponential model. To derive the same worst-case variability for Equations (12) and (13), we can generalise this approach, stating that

$$P(s_t < \Psi) = \int_0^{\Psi} \frac{1}{s_t \sigma_0 \sqrt{2\pi}} \exp\left\{\frac{-(\ln(s_t) + g(t) - \mu_0)^2}{2\sigma_0^2}\right\} ds_t = \varphi, \tag{14}$$

where $g(t)$ is some function of time t, and s_t is either of x_t or z_t. For the observable distribution, $g(t) = -\ln(\Theta_t)$, and for the total, $g(t) = \ln(A) - \ln(\Omega_t)$. Solving Equation (14) for $g(t)$ yields

$$g(t) = -\frac{1}{2}\sigma_0^2 + \sqrt{2}\sigma_0 \mathrm{erf}^{-1}(2\varphi - 1) + \ln\left(\frac{\overline{s_0}}{\Psi}\right), \tag{15}$$

where $\overline{s_0}$ is the pre-depuration arithmetic mean of the generalised NoV distribution. Equation (15) is of concave quadratic form with respect to σ_0, which is maximised when

$$\sigma_0 = \sqrt{2}\mathrm{erf}^{-1}(2\varphi - 1), \tag{16}$$

irrespective of the form of $g(t)$, and thus is equivalent to that derived in McMenemy et al. (2018), who defined this as the *worst-case variability* (WCV).

From all preceding statements, it can be shown that the arithmetic mean for the observable NoV load at time t is $\overline{x_t} = \Theta_t \overline{x_0}$, and the arithmetic mean of the total NoV load $P(z_t)$ can be shown to be $\overline{z_t} = \Omega_t \overline{z_0}$.

2.6. Salient depuration times

The assumption of a cryptic pathogen compartment (y_t) within the model results in the MDT for the total load being greater than that of the observable load only if $a \neq 0$. It is crucial to quantify this difference, as any cryptic NoV load could contribute to PCR test results under-reporting NoV, and also potentially result in an increased food safety risk. Fig. 2 shows the decays of the observable ($\overline{x_t}$) and total ($\overline{z_t}$) mean NoV loads, where it is apparent that some time must elapse in depuration before the total NoV load ($\overline{z_t}$) decays to equal the value of the initial, observable load ($\overline{x_0}$). Note also that $\overline{x_t}$ begins to closely approximate $\overline{z_t}$ after a significant time, being mainly dependent upon the value of the parameter A.

Three salient depuration times are shown in Fig. 2:

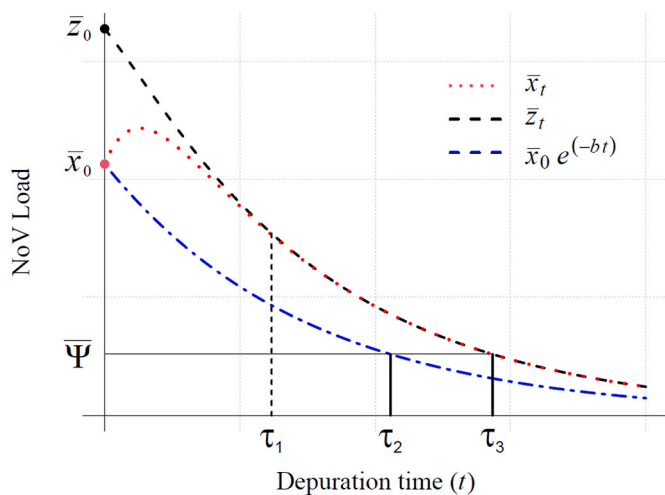τ_1: cryptic NoV load approaches zero, i.e., when $\overline{x_t} \approx \overline{z_t}$.

Fig. 2. Generic plot of dynamics of mean pathogen loads $\overline{x_t}$ (observable NoV load), $\overline{z_t}$ (total NoV load) assuming $A \neq 0$. The model described in (McMenemy et al., 2018) is shown here as $\overline{x_0}e^{-bt}$, with b the depuration rate.

We can identify the time (τ_1) when the mean, observable load closely approximates the mean, total NoV load. This is equivalent to when $y_t \to 0$, i.e., when almost all of the initial, cryptic NoV load (y_0) has transited to x_t (mathematically, $y_t \neq 0$; however, y_t could reduce to zero in reality). Setting a proportion p close to 1, ($p \lesssim 1$), we can calculate when τ_1 occurs, i.e., when $\overline{x_t} \approx \overline{z_t}$ or $\overline{y_{\tau_1}} = (1-p)\overline{y_0}$. This can be simplified using $\overline{y_{\tau_1}} = \overline{y_0}\exp\{-k\tau_1\}$ to obtain:

$$\tau_1 = -\frac{1}{k}\ln\{1-p\}. \tag{17}$$

τ_2: MDT of exponential model, $\overline{x_0}\exp\{-bt\} = \overline{\Psi}$.

A description of the arithmetic mean of a log-normal distribution satisfying both Ψ and φ control parameters (denoted by $\overline{\Psi}$) can be obtained from the definition of τ_2, and can be stated as

$$\overline{\Psi} = \overline{x_0}\exp\{-b\tau_2\}, \tag{18}$$

In McMenemy et al. (2018), MDTs were calculated from

$$T_{\mathrm{WCV}} = b^{-1}\left[\left(\mathrm{erf}^{-1}(2\varphi - 1)\right)^2 + \ln\left(\frac{\overline{x_0}}{\Psi}\right)\right]. \tag{19}$$

Adopting this same approach allows us to state τ_2, the MDT of the exponential model, as

$$\tau_2 = b^{-1}\left[\left(\mathrm{erf}^{-1}(2\varphi - 1)\right)^2 + \ln\left\{\frac{\overline{x_0}}{\Psi}\right\}\right], \tag{20}$$

τ_3: MDT of compartmental model, $\overline{z_t} = \overline{\Psi}$. The mean total pathogen load at any time t is defined as $\overline{z_t} = \Omega_t \overline{z_0}$. From this, and an examination of Fig. 2, it is apparent that the MDT for the total NoV load (here designated as τ_3) occurs when $\overline{z_{\tau_3}} = \overline{\Psi}$. Equation (6) ($z_t = z_0\Omega_t$) and 18 ($\overline{\Psi} = \overline{x_0}\exp\{-b\tau_2\}$) can be substituted in to obtain

$$\Omega_{\tau_3} = \frac{\Psi}{\overline{z_0}}\exp\left\{-\frac{1}{2}\sigma_0^2\right\}. \tag{21}$$

Here Ω_{τ_3} is a function of the mean, total NoV load's minimum depuration time (τ_3). We have previously shown that an analytical solution w.r.t. time t for Ω_t is not attainable; therefore, numerical methods must be used to obtain values for τ_3. The value of τ_3 obtained from Equation (21) is the MDT which accounts for both the observed and unobserved NoV loads present. It follows that the value of $\tau_3 - \tau_2$ quantifies the depuration time required to meet the NoV threshold value Ψ in addition to the MDT calculated when assuming no cryptic NoV loads.

3. Results

Comparisons between the dynamics of the compartmental model were made with those of the depuration model developed in McMenemy et al. (2018). The sensitivity of the compartmental model parameters was also analysed, with particular focus on the sensitivity of the internal pathogen transfer rate, k. Finally, and most importantly, differentials between the MDTs for the compartmental model (τ_3) and the exponential decay model (τ_2) were calculated and analysed.

3.1. Parameterization of compartmental model

McMenemy et al. (2018) parameterized their model from literature, obtaining values for b (depuration decay rate), Ψ (NoV limit) and $\overline{x_0}$ (initial mean NoV load) from literature (Doré et al., 2010; Lowther et al., 2012), and set $\varphi \in \{0.90, 0.95, 0.99\}$. We only used $\varphi = 0.95$ in our analysis to examine the differences between the depuration decay and compartmentalised models. To obtain a value for k, the internal transfer

rate of NoV from cryptic to observable compartments, we utilised longitudinal data obtained by Neish (2013), where they conducted PCR assay on oyster samples at depuration times $t \in \{0, 42, 90, 162, 210, 258, 330\}$ hours. These data were used to estimate parameter values for A, k, b and $\overline{x_0}$ using nonlinear least squares regression and values are shown in Table 1. B Appendix contains further details of the experiment and data.

The regression derived value of $\overline{x_0}$ shown in Table 1 is significantly greater than that of the value of $\overline{x_0}$ obtained from literature, and is due to the regression value being derived from oyster samples that were exposed to artificially high levels of effluence before depuration to ensure that all samples would return NoV values above the limit of quantitation.

3.2. Comparison of initial distributions

Equations (4)–(7) and (10) and (11) model the depuration dynamics of NoV within oysters, providing descriptions of both the observable and cryptic compartments across a population of oysters. If any cryptic NoV load exists at the pre-depuration stage (i.e., $A \neq 1$ when $t = 0$) then the pre-depuration distributions of the observable and total NoV loads would exhibit different shapes.

Fig. 3a shows the distribution of the observable compartment, $P(x_0)$, and exhibits a positive skewness and a peak close to zero. These contribute to the probability $p = 0.423$ of the observable distribution's population that will have a NoV load less than $\Psi = 200$ NoV cpg. Fig. 3b plots the total NoV load at pre-depuration ($P(z_0)$), and we observed a notably smaller peak than that of $P(x_0)$. This is due to the addition of the cryptic NoV compartment to the model, resulting in a flattening of the PDF towards higher values for all variates. As the mode is much smaller than that of $P(x_0)$, this reduces the area between $0 < z_0 < 200$ while increasing the area of the tail ($z_0 > 1000$). These plots conform with sensible expectations: the inclusion of additional, sequestered NoV loads per oyster should result in an across-the-board increase in the total pathogen load.

3.3. Sensitivity of salient times to parameters

The sensitivity of each of the salient times to variation in the four parameters A, b, k and p is shown in Fig. 4. In each plot, one of four

Table 1
Parameters and values derived from literature and nonlinear least squares regression. The salient times impacted by changes in parameters values are also noted.

Parameter	Literature value	Regression value [c]	Parameter value applied	Salient time impacted
Initial observable NoV proportion, A	N/A	0.461	0.461	τ_3
Depuration decay rate, b	0.01339 [a]	0.00398	0.01339	τ_2, τ_3
Internal NoV transfer rate, k	N/A	0.07453	0.07453	τ_1, τ_3
Pre-depuration mean NoV load, $\overline{x_0}$	1064 [b]	191245	1064	τ_2, τ_3
NoV assurance level, φ	0.95	N/A	0.95	τ_2, τ_3
Log-normal distribution location, μ_0	5.617	N/A	5.617	τ_2, τ_3
Log-normal distribution spread, σ_0	1.645	N/A	1.645	τ_2, τ_3
NoV threshold limit, Ψ	200	N/A	200	τ_2, τ_3
Proportion for when $\overline{y_t} \approx 0$, p	N/A	N/A	0.99	τ_1

[a] (Doré et al., 2010).
[b] (Lowther et al., 2012).
[c] Values obtained from (Neish, 2013) using 'nls' function in R (R Core Team, 2013).

variables is varied while holding all other parameters fixed, with the process repeated for each of A, b, k and p. Lines show the impact of varying each parameter $\pm 1/3$ of the value stated in Table 1, with the exception of p where, to allow $\pm 1/3$ sensitivity analysis, $p = 0.75$ was used.

Fig. 4a shows how the value of τ_1 is impacted by varying one parameter at a time, with only changes to k and p affecting the value of τ_1 (cf. Equation (17)). Fig. 4b, as expected from Equation (20), shows that only changes to b would impact the value of τ_2. Fig. 4c provides valuable information regarding k, the internal transfer rate of NoV from the cryptic compartment to the observable compartment. Other than the regression value of k previously derived from data ((Neish, 2013)), no other estimations of this parameter exist. Observing that varying $0.07453 \pm 1/3$ makes minimal difference to the value of τ_3 provides our model with a viable estimation of k; however, we need to check the behaviour of k for values outside this range.

Fig. 5a shows the sensitivity of τ_3 to changes in b and k across the range (0,1). We earlier discussed whether the feasibility of $b > k$ is biologically relevant, and therefore only the top left triangle of both figures (values above the $b = k$ line) applies. When either of $b, k \to 0$, it is seen that $\tau_3 \to \infty$, and when both $b, k \to 1$ we see $\tau_3 \to 0$.

Fig. 5b, shows the behaviour of $\tau_3 - \tau_2$, i.e., the additional minimum depuration time required when the cryptic NoV loads are taken into account ($A = 0.461$). Fig. 5a has a minimum at (0.5, 0.5); however, Fig. 5b shows a minimum at ($\approx$0.35, 0.5). Why this occurs is beyond the remit of this paper as our focus is on the modelling of NoV likely sequestered in cryptic compartments; however, we invite the reader to investigate why this minimum occurs in this space.

Industry stakeholders have little or no control over the internal transfer parameter k; its value is a consequence of the biology of the oysters being depurated and possibly the temperature and flow rate of the water during depuration. The value we have obtained by regression from the Neish data ($k = 0.07453$) is highlighted in Fig. 5b, along with the depuration decay rate obtained from literature ($b = 0.01339$). Where these lines cross in Fig. 5b show that a minimum depuration time of approximately 100 h would be required to satisfy the control parameter values of $\Psi = 200$ NoV cpg and $\varphi = 0.95$. Both values of b and k would need to be significantly increased to reduce depuration times although, as a minimum of 42 h in depuration is currently required by law, they would only need to be increased by a small factor.

3.4. MDT comparison between models

Fig. 4c showed that varying parameters A, b and k impact τ_3, the MDT of the compartmental model, with changes to the depuration decay rate b causing the largest change in the magnitude of τ_3. Fig. 6a and Table 2a highlight how salient times are affected by increasing the value of A, decaying from $\tau = 757$ h when $A \approx 0$, to 226 h when $A = 1$.

Comparing the sensitivity of τ_3 to changes in k (cf. Fig. 6b, Table 2b) to that observed in Fig. 6c and Table 2c, we see that factoring down the decay rates of our base values for $k^* = 0.07453$ and $b^* = 0.01339$ has markedly different impacts on the $\tau_3 - \tau_2$ values. However, this is only a consequence of the gradients of the MDTs at the locations of k^* and b^*, where b^* is located at a steeper location than k^*. We also observed that the depuration model decays more quickly than the compartmental model, a consequence of the inclusion of the cryptic NoV compartment in that model, and that the change in the MDT τ_2 is inversely proportional to the change in the depuration decay rate b.

4. Discussion and conclusions

The compartmental model described here extends the authors' exponential depuration model, as detailed in (McMenemy et al., 2018), that describes the dynamics of NoV in shellfish populations. That depuration model has been extended by an assumption of internal sequestration of pathogens within individual oysters, splitting the pathogen

(a) Initial observable distribution, $P(x_0)$ (b) Initial total distribution, $P(z_0)$
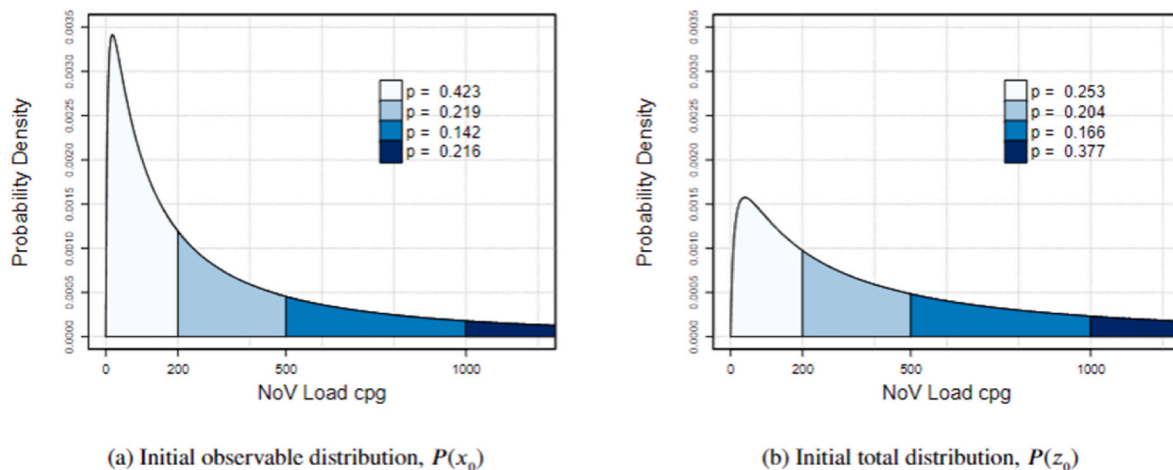
Fig. 3. Parameters used: $\mu_0 = 5.617$, $\sigma_0 = 1.645$ and $\overline{x_0} = 1064$ NoV cpg, with the proportion of observable NoV $A = 0.461$. Distributions are shown in four tranches: $0 < x_0 < 200$, $200 < x_0 < 500$, $500 < x_0 < 1000$ and $x_0 > 1000$. p values are the probability of a randomly selected oyster having a NoV load in that particular segment.

(a) τ_1 sensitivity analysis   (b) τ_2 sensitivity analysis   (c) τ_3 sensitivity analysis
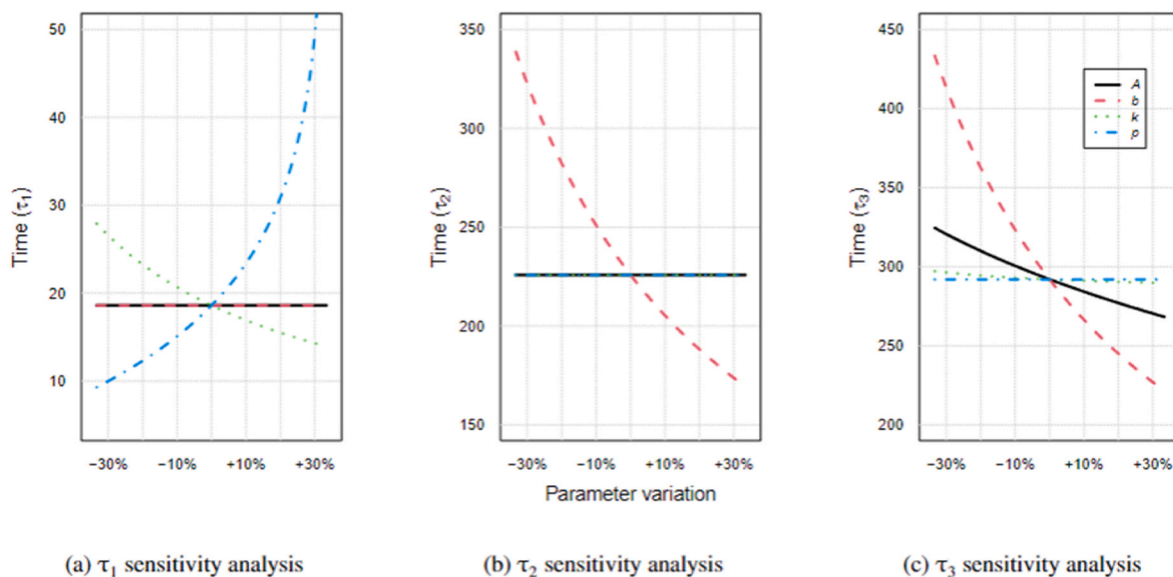
Fig. 4. Sensitivity analysis of parameters within the compartmental model. Initial parameter values are: $A = 0.461$, $b = 0.01339$, $k = 0.07453$, $p = 0.75$, with other parameters fixed at $\overline{x_0} = 1064$ cpg, $\Psi = 200$ cpg, $\varphi = 0.95$

load into cryptic and observable compartments. This approach has been undertaken based on evidence in the literature that shows that NoV loads are not solely located in the digestive gland but are found distributed throughout each animal's anatomy. Parameterization of the compartmental model has been based in part on values from the depuration model from McMenemy et al. (2018), as well as reasonable estimates for k and A from regression techniques applied to the Neish data (Neish, 2013), and that the value of p should be $\lesssim 1$. The value of the internal transfer rate k stated in Table 1 must conform to $b < k$ for biological reasons, and is due to the fact that, if $b \geqslant k$, then the digestive gland (compartment x_t in the compartmental model) would not be the primary initial repository of NoV, which is contrary to literature findings (Doré and Lees, 1995; Wang et al., 2008). The sensitivity analysis carried out here showed that the impact of k upon any of the salient times τ_i is very limited, inducing only small variation in the values of τ_1, τ_2 and τ_3. This is significant to our methodology here as, in the absence of being able to obtain reliable estimates of k, we have had to rely upon indirect methods to derive a parameter value for k, and any inaccuracies in our estimate of k would only result in small changes to the model's results.

The use of only one cryptic and one observable compartment of NoV, as well as a constant value of k, could be superseded if future longitudinal, empirical studies could quantify NoV levels within more distinct tracts of the oyster's physiology.

The significant outcome of this model is the increase in the length of the MDT required due to inclusion of an initial cryptic load. This increase in MDT due to compartmentalisation of NoV away from the observable, quantifiable load, represented by $(\tau_3 - \tau_2)$ in our model, is shown to be most responsive to changes in the value of A, the proportion of initial NoV loads which are observable to current testing practices. Fig. 4 shows that, for low values of A, MDTs of τ_3 are much greater than those of τ_2 (the MDT assuming no cryptic NoV loads at pre-depuration). Only as $A \to 1$ do we observe the MDTs of the total NoV load approach the MDT using the exponential model (cf. Table 2a). Further studies are required to validate our modelling of NoV compartmentalisation in oysters similar to that of the Neish study (Neish, 2013), ideally with more replicates per time sample and more time points sampled. This would provide finer granularity of the data across time, and more samples would allow more precision in aggregating each time point's
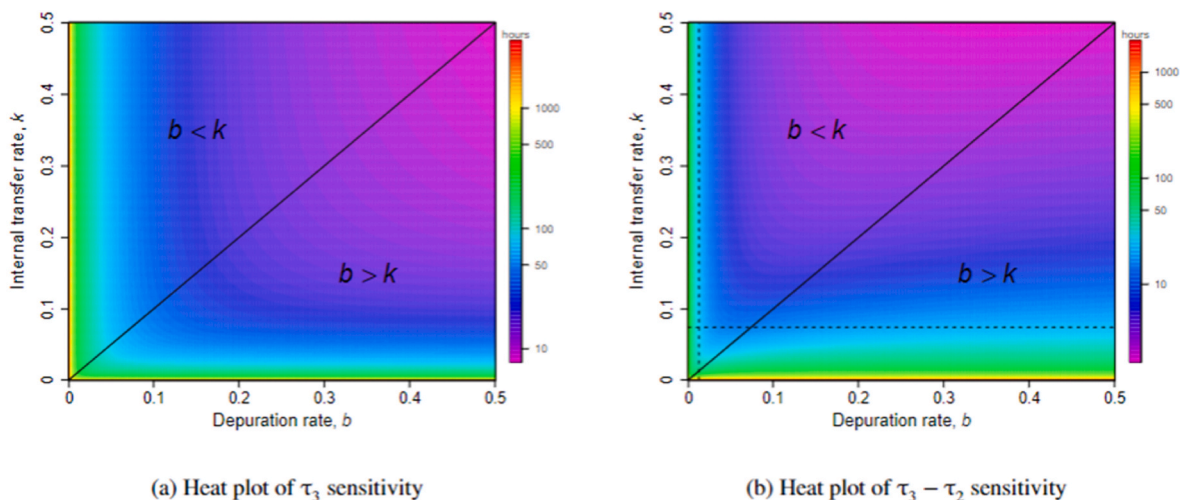
(a) Heat plot of τ_3 sensitivity

(b) Heat plot of $\tau_3 - \tau_2$ sensitivity

Fig. 5. Heat plots of b and k sensitivity in compartmental model. Other parameter values fixed at: $A = 0.461$, $p = 0.99$, $\overline{x_0} = 1064$ cpg, $\Psi = 200$ cpg, $\varphi = 0.95$. Vertical dashed line highlights $b = 0.01339$, and horizontal dash when $k = 0.07453$. Note that the z-values of the plot are shown on a $\log_{10}$ scale (in hours).

(a) Minimum depuration time, τ_3 vs initial observable NoV load proportion, A

(b) Minimum depuration time, τ_3 vs internal transfer rate k; $k^* = 0.07453$

(c) Minimum depuration times, τ_2, τ_3 vs depuration decay rate b; $b^* = 0.01339$
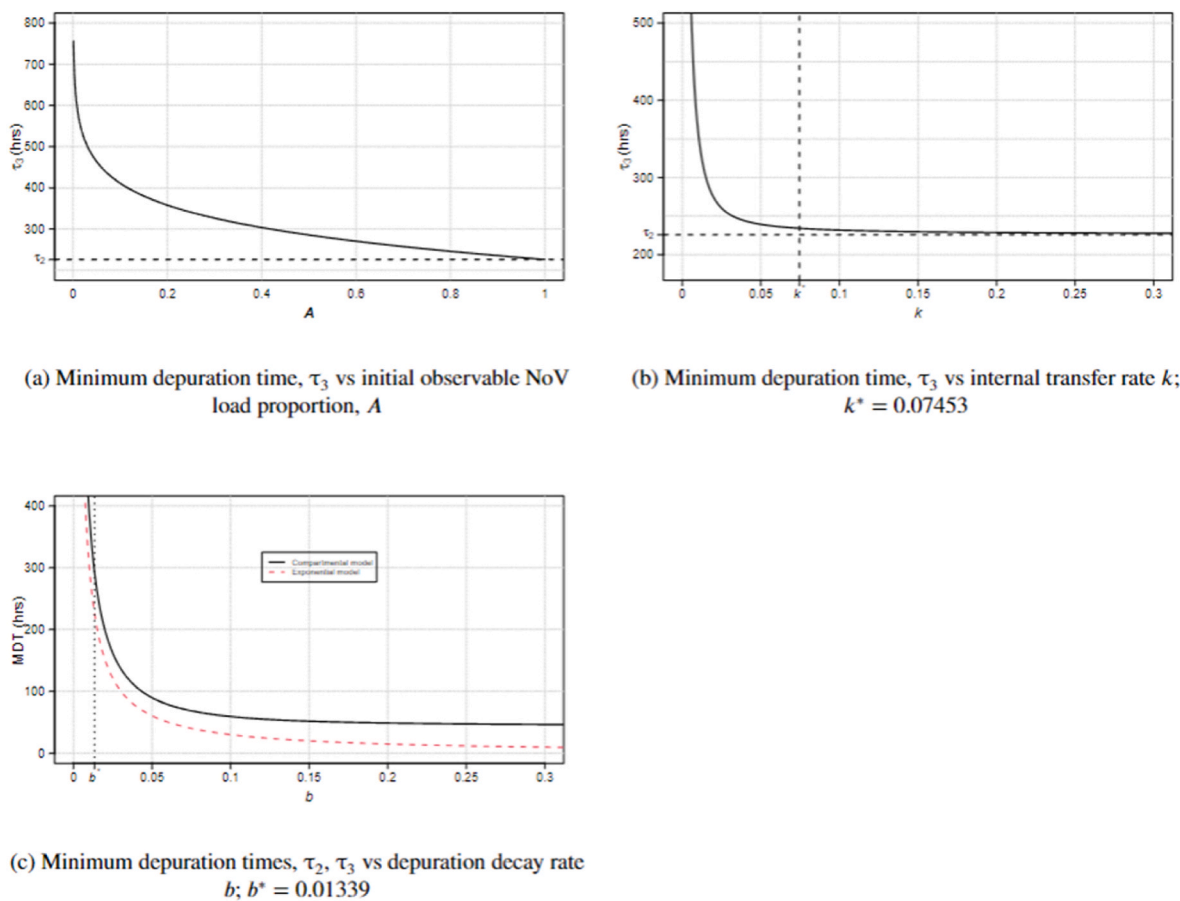
Fig. 6. Comparison of minimum depuration times when: 6a) the proportion of observable of NOV load per oyster is varied; 6b) the internal NoV tranfer rate (k) is varied; 6c) the depuration decay rate is varied. Other model parameters are fixed at: $b = 0.01339$ (), $k = 0.07453$ (), $A = 0.461$ (), $\overline{x_0} = 1064$ NoV cpg, $\Psi = 200$ NoV cpg, $\varphi = 0.95$, $p = 0.99$.

data.

Not only does this compartmental model show that internal NoV compartmentalisation should be considered, but it also indicates that the timing of pathogen detection testing should also be considered with respect to the levels of potential pathogens in the local water of the harvested shellfish. At present there is no pathogen testing during or after depuration; testing is done at periods throughout the year to classify the water and determine whether depuration is needed. Therefore, under many circumstances, current depuration times are unlikely to be long enough to reduce total NoV loads to reasonable levels, and the additional insight from this study suggests that these need to be longer than were previously estimated in (McMenemy et al., 2018) due to the

Table 2
Impact upon salient times τ_1 (cryptic NoV load is approx. zero), τ_2 (MDT of exponential model) and τ_3 (MDT of compartmental model) when: 2a) the initial observable proportion of NoV load, A, is varied; 2b) the internal transfer rate, k, is varied; and 2c) the depuration decay rate, b, is varied.

(a) Salient times when varying A, the proportion of initial observable NoV load						
A	0.5	0.6	0.7	0.8	0.9	1.0
τ_1	62	62	62	62	62	62
τ_2	226	226	226	226	226	226
τ_3	285	270	257	246	235	226
$\tau_3 - \tau_2$	59	44	31	20	9	0

(b) Salient times when internal transfer rate, k, is varied ($k = 0.07453$)						
k	$0.1k$	$0.25k$	$0.5k$	k	$2k$	$3k$
τ_1	618	247	124	62	31	21
τ_2	226	226	226	226	226	226
τ_3	535	341	303	292	288	286
$\tau_3 - \tau_2$	309	115	77	66	62	60

(c) Salient times when depuration decay rate, b, is varied ($b = 0.01339$)						
b	$0.1b$	$0.25b$	$0.5b$	b	$2b$	$3b$
τ_1	62	62	62	62	62	62
τ_2	2259	903	452	226	113	75
τ_3	2844	1142	575	292	152	106
$\tau_3 - \tau_2$	585	239	123	66	39	31

cryptic levels. However, further validation of our model and associated assumptions would be required before any testing recommendations were to be made to legislators and industry stakeholders.

If protocols, similar to those for the mitigation of *E. coli*, were to be introduced to mitigate NoV levels within shellfish, then the timing of sample testing for NoV would be vital. Based on this model's results, pre-

depuration testing would not detect any cryptic NoV loads present; therefore, either during or post-depuration NoV testing would be optimal for the detection of total NoV loads present. The results here show that it would take approximately 62 h for any cryptic NoV loads to dissipate (cf. Table 2); therefore, any during or post-depuration NoV testing should be undertaken after this time point in the depuration process.

Credit author statement

Declaration of competing interest

The authors declare that they have no known competing financial interests or personal relationships that could have appeared to influence the work reported in this paper.

Acknowledgements

A Appendix

The first order, homogeneous equations describing NoV compartmentalisation allow analytic solutions to be obtained for Equations (1) and (2) and z_t. Firstly, using separation of variables and $x_0 = Az_0$, an analytical solution for the unobservable compartment y_t is obtained:

$$y_t = \frac{1-A}{A}x_0 \exp\{-kt\}. \tag{22}$$

Substituting Equation (22) into Equation (1) then applying an integrating factor (of $\exp\{bt\}$) allows an analytical solution for x_t to be obtained where

$$x_t = x_0\, \Theta_t, \tag{23}$$

$$\Theta_t = A^{-1}\left[\frac{k(1-A)}{(b-k)}\exp\{-kt\} + \frac{(Ab-k)}{(b-k)}\exp\{-bt\}\right], \tag{24}$$

and $0 \leqslant A \leqslant 1$, $b \neq k$.

If $k < b$, there would be no accumulation of NoV in x_t, which is contrary to literature findings that state NoV selectively binds and aggregates within the digestive gland of molluscs (x_t) (Le Guyader et al., 2006; Ueki et al., 2007; Anonymous, 2012). Therefore, we are restricted to applying $b < k$ to describe the internal transfer of NoV from y_t into x_t compartment.

An analytical solution for the total NoV load in an oyster (z_t) is also obtained by substituting the equations describing x_t and y_t (Equations (22)–(24)) into $z_t = x_t + y_t$ and simplifying to obtain

$$z_t = z_0\, \Omega_t, \tag{25}$$

where

$$\Omega_t = \left[\frac{b(1-A)}{(b-k)}\exp\{-kt\} + \frac{(Ab-k)}{(b-k)}\exp\{-bt\}\right]. \tag{26}$$

B Appendix

Neish conducted research in 2013 to determine whether variations in depuration water temperature and/or water treatment would have a

significant impact upon the decay rate of NoV in shellfish (Neish, 2013). The study compared the effectiveness of depuration water temperatures of 8 °C versus 16 °C, and ultraviolet radiation versus ozone as disinfectants of depuration tank water. Fig. 7 shows the data from one of the experiments carried out using ultraviolet radiation water treatment and tank water with a temperature of 16 °C.
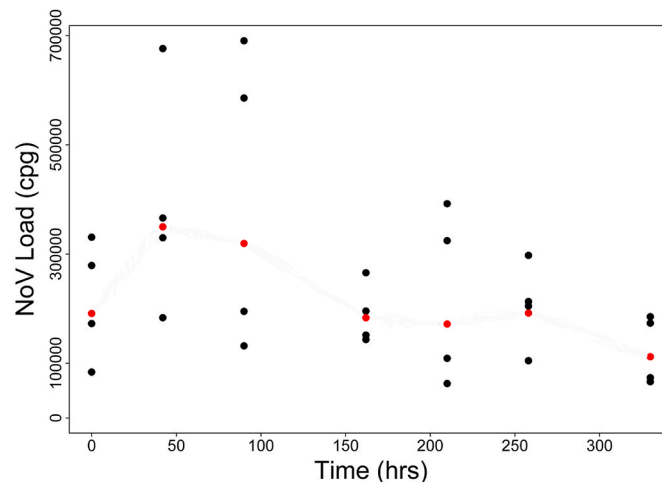

Fig. 7. Plot of during depuration dataset with water temperature of 16 °C. Four homogenates, each comprised of ten oysters, were tested for genotype II NoV loads at $t = 0$, 42, 90, 162, 210, 258, 330 h and are shown on the plot as black points. Red points indicate geometric mean of each time point's data

The data showed that depuration water temperature of 16 °C was statistically more effective than water at 8 °C, although still only showed a slight improvement in NoV levels after 330 h. The study also noted that ozone did not significantly improve NoV mitigation compared with the use of ultraviolet irradiation. Neish's data were obtained by PCR assay of four sets of 10-mollusc homogenates of *Magellana gigas*, at seven time points across a period of depuration. The first time point was a pre-depuration measure, with the second NoV sample taken after 42 h - the minimum depuration time required by regulation for class B harvested shellfish. Further samples were taken at 90, 162, 210, 258 and 330 respectively, and PCR assay was carried out on all samples.

Fig. 7 shows that an increase in the geometric means of NoV levels between 0 and 42 h was recorded by the study for the 16 °C data. This increase can be attributed to an internal transfer of NoV load from a compartment of the oyster, that currently cannot be assayed, into the digestive glands of the oyster, the only section of the oyster which is currently tested by PCR.

References

Anonymous, 2004. Regulation (EC) No. 854/2004 of the European Parliament and of the Council of 29 April 2004 Laying Down Specific Rules for the Organisation of Official Controls on Products of Animal Origin Intended for Human Consumption. Official Journal of the European Union, pp. 155–206.

Anonymous, 2012. Scientific opinion on norovirus (NoV) in oysters: methods, limits and control options. EFSA J. 10 (1), 1–39. https://doi.org/10.2903/j.efsa.2012.2500. Available.

Anonymous, 2017. Microbiology of the food chain—horizontal method for determination of hepatitis A virus and norovirus using real-time RT-PCR—Part 1: method for quantification. In: Tech. Rep. International Organization for Standardization, Geneva. ISO 15216-1:2017.

Armitage, R., 2022. Sewage in UK waters: a raw deal for wild swimmers. Br. J. Gen. Pract. 72 (723), 486–487. https://doi.org/10.3399/bjgp22X720833.

Bányai, K., Estes, M.K., Martella, V., Parashar, U.D., 2018. Viral gastroenteritis. Lancet 392 (10142), 175–186. https://doi.org/10.1016/S0140-6736(18)31128-0.

Brown, D., 2020. Sewage Discharged into Rivers 400,000 Times. https://www.bbc.co.uk/news/science-environment-56590219. accessed: 2022-12-15 (2021).

Doré, W.J., Lees, D.N., 1995. Behavior of Escherichia coli and male-specific bacteriophage in environmentally contaminated bivalve molluscs before and after depuration. Appl. Environ. Microbiol. 61 (8), 2830–2834. https://doi.org/10.1128/aem.61.8.2830-2834.1995.

Doré, B., Keaveney, S., Flannery, J., Rajko-Nenow, P., 2010. Management of health risks associated with oysters harvested from a norovirus contaminated area, Ireland, February-March 2010. Euro Surveill. 15 (19) https://doi.org/10.2807/ese.15.19.19567-en pii/19567.

Esposito, S., Ascolese, B., Senatore, L., Codecà, C., 2014. Pediatric norovirus infection. Eur. J. Clin. Microbiol. Infect. Dis. 33, 285–290. https://doi.org/10.1007/s10096-013-1967-9.

Food Standards Agency, 2022. Shellfish Classification, Tech. Rep. Food Standards Agency accessed: 2023-01-13. https://www.food.gov.uk/business-guidance/shellfish-classification.

Greening, G.E., McCoubrey, D.J., 2010. Enteric viruses and management of shellfish production in New Zealand. Food Environ. Virol. 2, 167–175. https://doi.org/10.1007/s12560-010-9041-6.

Guyader, F.S.L., Bon, F., DeMedici, D., Parnaudeau, S., Bertone, A., Crudeli, S., Doyle, A., Zidane, M., Suffredini, E., Kohli, E., Maddalo, F., Monini, M., Gallay, A., Pommepuy, M., Pothier, P., Ruggeri, F.M., 2006. Detection of multiple noroviruses associated with an international gastroenteritis outbreak linked to oyster consumption. J. Clin. Microbiol. 44, 3878–3882. https://doi.org/10.1128/JCM.01327-06.

Hassard, F., Sharp, J.H., Taft, H., LeVay, L., Harris, J.P., McDonald, J.E., Tuson, K., Wilson, J., Jones, D.L., Malham, S.K., 2017. Critical review on the public health impact of norovirus contamination in shellfish and the environment: a UK perspective. Food Environ. Virol. 9 (2), 123–141. https://doi.org/10.1007/s12560-017-9279-3.

Kambhampati, A.K., Wikswo, M.E., Barclay, L., Vinjé, J., Mirza, S.A., Rei, E., Sabina, B., Beggs, J., Riner, D.K., Cebelinski, E., Saupe, A., Bartling, A., Loeck, B.K., Chase, N., Houston, J., Brandt, E., Salehi, E., DeBess, E., Tsaknaridis, L., Goodwin, G., Mohamed, H., Golwalkar, M., Thomas, L., Donnelly, M.K., Greene, H., Davis, T., Roberts, L., Christensen, R., Peterson, M., 2022. Notes from the field: norovirus outbreaks reported through NoroSTAT — 12 states, August 2012–July 2022. MMWR. Morbidity and Mortality Weekly Report 71 (38), 1222–1224. https://doi.org/10.15585/mmwr.mm7138a3.

Keaveney, S., Rupnik, A., Fitzpatrick, A., Devilly, L., Fahy, J., Doré, B., 2022. Impact of COVID-19 nonpharmaceutical interventions on the extent of norovirus contamination in oyster production areas in Ireland during winter 2020 to 2021. J. Food Protect. 85 (10), 1397–1403. https://doi.org/10.4315/JFP-22-031.

Laville, S., McIntyre, N., 2019. Water Firms Discharged Raw Sewage into England's Rivers 200,000 Times. https://www.theguardian.com/environment/2020/jul/01/water-firms-raw-sewage-england-rivers. accessed: 2022-12-15 (2019).

Le Guyader, F.S., Loisy, F., Atmar, R.L., Hutson, A.M., Estes, M.K., Ruvoën-Clouet, N., Pommepuy, M., Le Pendu, J., 2006. Norwalk virus-specific binding to oyster digestive tissues. Emerg. Infect. Dis. 12 (6), 931–936. https://doi.org/10.3201/eid1206.051519.

Leduc, A., Leclerc, M., Challant, J., Loutreul, J., Robin, M., Maul, A., Majou, D., Boudaud, N., Gantzer, C., 2020. F-specific RNA bacteriophages model the behavior of human noroviruses during purification of oysters: the main mechanism is probably inactivation rather than release. Appl. Environ. Microbiol. https://doi.org/10.1128/AEM.

Lees, D., 2000. Viruses and bivalve shellfish. Int. J. Food Microbiol. 59, 81–116. https://doi.org/10.1016/S0168-1605(00)00248-8.

Lees, D.N., 2010. International standardisation of a method for detection of human pathogenic viruses in Molluscan shellfish. Food Environ. Virol. 2 (3), 146–155. https://doi.org/10.1007/s12560-010-9042-5.

Loisy, F., Atmar, R.L., Guillon, P., Le Cann, P., Pommepuy, M., Le Guyader, F.S., 2005. Real-time RT-PCR for norovirus screening in shellfish. J. Virol Methods 123 (1), 1–7. https://doi.org/10.1016/j.jviromet.2004.08.023.

Lowther, J.A., Gustar, N.E., Powell, A.L., O'Brien, S., Lees, D.N., 2018. A one-year survey of norovirus in UK oysters collected at the point of sale. Food Environ. Virol. 10 https://doi.org/10.1007/s12560-018-9338-4.

Lowther, J.A., Gustar, N.E., Powell, A.L., Hartnell, R.E., Lees, D.N., 2012. Two-year systematic study to assess norovirus contamination in oysters from commercial harvesting areas in the United Kingdom. Appl. Environ. Microbiol. 78 (16), 5812–5817. https://doi.org/10.1128/AEM.01046-12.

Ma, L., Liu, H., Su, L., Zhao, F., Zhou, D., Duan, D., 2018. Histo-blood group antigens in Crassostrea gigas and binding profiles with GII.4 Norovirus. J. Oceanol. Limnol. 36, 1383–1391. https://doi.org/10.1007/s00343-018-7024-x.

McMenemy, P., Kleczkowski, A., Lees, D.N., Lowther, J., Taylor, N., 2018. A model for estimating pathogen variability in shellfish and predicting minimum depuration times. PLoS One 13 (3), e0193865. https://doi.org/10.1371/journal.pone.0193865.

Muniain-Mujika, I., Girones, R., Tofiño-Quesada, G., Calvo, M., Lucena, F., 2002. Depuration dynamics of viruses in shellfish. Int. J. Food Microbiol. 77, 125–133. https://doi.org/10.1016/S0168-1605(02)00052-1.

Neish, A., 2013. Cefas contract report C5224: investigative trials on the purification of oysters to identify ways of reducing norovirus. Cefas. Tech. rep.

O'Brien, S.J., Sanderson, R.A., Rushton, S.P., 2018. Control of norovirus infection. Curr. Opin. Gastroenterol. 35 (1), 14–19. https://doi.org/10.1097/MOG.0000000000000491.

Patel, M.M., Widdowson, M.-A., Glass, R.I., Akazawa, K., Vinjé, J., Parashar, U.D., 2008. Systematic literature review of role of noroviruses in sporadic gastroenteritis. Emerg. Infect. Dis. 14, 1224–1231. https://doi.org/10.3201/eid1408.071114.

Polo, D., Feal, X., Varela, M.F., Monteagudo, A., Romalde, J.L., 2014. Depuration kinetics of murine norovirus in shellfish. Food Res. Int. 64, 182–187. https://doi.org/10.1016/j.foodres.2014.06.027.

Polo, D., Feal, X., Romalde, J.L., 2015. Mathematical model for viral depuration kinetics in shellfish: an useful tool to estimate the risk for the consumers. Food Microbiol. 49, 220–225. https://doi.org/10.1016/j.fm.2015.02.015.

Pouillot, R., Smith, M., Van Doren, J.M., Catford, A., Holtzman, J., Calci, K.R., Edwards, R., Goblick, G., Roberts, C., Stobo, J., White, J., Woods, J., DePaola, A., Buenaventura, E., Burkhardt, W., 2021. Risk assessment of norovirus illness from consumption of raw oysters in the United States and in Canada. Risk Anal. 42, 344–369. https://doi.org/10.1111/risa.13755.

R Core Team, R., 2013. A Language and Environment for Statistical Computing. R Foundation for Statistical Computing, Vienna, Austria, 3-900051-07-0. http://www.R-project.org/.

Rowan, N.J., 2023. Current decontamination challenges and potentially complementary solutions to safeguard the vulnerable seafood industry from recalcitrant human norovirus in live shellfish: quo Vadis? Sci. Total Environ. 874, 162380 https://doi.org/10.1016/j.scitotenv.2023.162380.

Rupnik, A., Doré, W., Devilly, L., Fahy, J., Fitzpatrick, A., Schmidt, W., Hunt, K., Butler, F., Keaveney, S., 2021. Evaluation of norovirus reduction in environmentally contaminated pacific oysters during laboratory controlled and commercial depuration. Food Environ. Virol. 13, 229–240. https://doi.org/10.1007/s12560-021-09464-2.

Savini, G., Casaccia, C., Barile, N.B., Paoletti, M., Pinoni, C., 2009. Norovirus in bivalve molluscs: a study of the efficacy of the depuration system. Vet. Ital. 45 (4), 535–539.

Schaeffer, J., Le Saux, J.C., Lora, M., Atmar, R.L., Le Guyader, F.S., 2013. Norovirus contamination on French marketed oysters. Int. J. Food Microbiol. 166 (2), 244–248. https://doi.org/10.1016/j.ijfoodmicro.2013.07.022.

Schaeffer, J., Treguier, C., Piquet, J.C., Gachelin, S., Cochennec-Laureau, N., Le Saux, J.C., Garry, P., Le Guyader, F.S., 2018. Improving the efficacy of sewage treatment decreases norovirus contamination in oysters. Int. J. Food Microbiol. 286 (May), 1–5. https://doi.org/10.1016/j.ijfoodmicro.2018.07.016.

Su, L., Ma, L., Liu, H., Zhao, F., Su, Z., Zhou, D., 2018. Presence and distribution of histo-blood group antigens in pacific oysters and the effects of exposure to noroviruses GI.3 and GII.4 on their expression. J. Food Protect. 81, 1783–1790. https://doi.org/10.4315/0362-028X.JFP-18-074.

Thongprachum, A., Khamrin, P., Chan-It, W., Malasao, R., Chaimongkol, N., Okitsu, S., Mizuguchi, M., Maneekarn, N., Hayakawa, S., Ushijima, H., 2013. Emergence of norovirus GII/4 2006a and 2006b variants in hospitalized children with acute gastroenteritis in Thailand. Clin. Lab. 59 (3–4), 271–276. https://doi.org/10.7754/Clin.Lab.2012.120316.

Ueki, Y., Shoji, M., Suto, A., Tanabe, T., Okimura, Y., Kikuchi, Y., Saito, N., Sano, D., Omura, T., 2007. Persistence of caliciviruses in artificially contaminated oysters during depuration. Appl. Environ. Microbiol. 73 (17), 5698–5701. https://doi.org/10.1128/AEM.00290-07.

van Beek, J., Ambert-Balay, K., Botteldoorn, N., Eden, J.S., Fonager, J., Hewitt, J., Iritani, N., Kroneman, A., Vennema, H., Vinjé, J., White, P.A., Koopmans, M., 2013. NoroNet, Indications for worldwide increased norovirus activity associated with emergence of a new variant of genotype II.4, late 2012. Euro Surveill. 18 (1), 8–9. https://doi.org/10.2807/ese.18.01.20345-en.

Wang, D., Wu, Q., Kou, X., Yao, L., Zhang, J., 2008. Distribution of norovirus in oyster tissues. J. Appl. Microbiol. 105 (6), 1966. https://doi.org/10.1111/j.1365-2672.2008.03970.x. –72.

Paul McMenemy is currently a Research Associate at the University of Strathclyde, where he is working on a number of projects, looking into understanding the spread of plant diseases, with focus on tree (ash dieback) and potato (blackleg). Paul obtained his PhD in Mathematics at the University of Stirling, modelling pathogens in shellfish, and worked there as a lecturer before moving to the University of Strathclyde. He has published research in diverse fields such as operations research, combinatorial and multi-objective optimisation, with particular expertise in epidemiology modelling.

Since obtaining his Theoretical Physics PhD from the Jagiellonian University in Poland in 1989, Adam has been working on Mathematical Biology, applying models to study human, animal and plant diseases, soil and terrestrial biodiversity, and climate change. He also has worked on parameter estimation for ecological and epidemiological systems. After a post-doctoral post in Germany, he came to Cambridge in 1992 to work on human and plant diseases. In 2007 he moved to Stirling and in 2018 he joined the University of Strathclyde as a Global Talent Chair. His recent work has been on bioeconomic modelling of crop and tree diseases, linking supply of pollination services to pesticide use, and addressing food security and sustainability in aquaculture, with funding coming from MRC, European Investment Bank, BBSRC, NERC, Scottish Government and Defra. He was part of the Expert Group that provided advice to the Scottish Government on the business case for the Plant Health Centre and is now a member of the Science Advice and Response Team for the Centre.

Nick Taylor is a renowned scientist who is currently working as Deputy Director of the Office for National Statistics. Before that, Nick was part of the Covid-19 taskforce in the United Kingdom, working closely in providing scientific advice to the UK Cabinet Office during the pandemic. Nick obtained his PhD in Epidemiology at the University of Stirling and worked for many years as the principal epidemiologist at Cefas, where his research interests focused on identifying and understanding risk factors influencing the establishment, spread, population dynamics and impact of aquatic pathogens, with a view to informing surveillance and control strategies. He also led the Aquatic Health Management Science Group, managing modellers, analysts, as well as field and laboratory scientists, in aquatic health research.